

A cylindrical expansion of the audio sound for a steerable parametric array loudspeaker

Jiaxin Zhong,^{1,a)} Ray Kirby,^{1,b)} Mahmoud Karimi,^{1,c)} and Haishan Zou^{2,d)}

¹Centre for Audio, Acoustics and Vibration, University of Technology, Sydney, New South Wales 2007, Australia

²Key Laboratory of Modern Acoustics and Institute of Acoustics, Nanjing University, Nanjing 210093, China

ABSTRACT:

In this work, a cylindrical expansion for the audio sound generated by a steerable baffled parametric array loudspeaker (PAL) based on the phased array technique is derived from the Westervelt equation. The expansion is a series of twofold summations with uncoupled angular and radial components in the cylindrical coordinate system. The angular component is determined by the trigonometric functions, and the radial component is an integral containing the Bessel functions and an arbitrary excitation velocity profile. The numerical results for a typical steerable PAL are presented and compared to those obtained using the convolution model. It is found that the prediction of the audio sound using the proposed cylindrical expansion improves the agreement with the experimental results when compared to the existing models. This is because no further approximations are required in the cylindrical expansion of the quasilinear solution of the Westervelt equation, whereas the complex near field nonlinear interactions between the ultrasonic waves cannot be correctly captured in a convolution model. The proposed cylindrical expansion does, therefore, provide an alternative approach to modeling a phased array PAL and high accuracy with a relatively low computational cost. © 2021 Acoustical Society of America.

<https://doi.org/10.1121/10.0007280>

(Received 30 August 2021; revised 26 October 2021; accepted 26 October 2021; published online 18 November 2021)

[Editor: Sean F. Wu]

Pages: 3797–3806

I. INTRODUCTION

Parametric array loudspeakers (PALs) have been widely used in many scenarios because of their ability to generate highly directional audio sound at low frequencies.¹ The physical mechanism for the PAL is that the directional audio sound beam is generated by the nonlinear interactions between the ultrasound beams radiated by an array of ultrasonic transducers.² For a conventional PAL, the excitation velocity profile for the ultrasound is uniform on the radiation surface such that the mainlobe of the radiation pattern lies on the radiation axis of the PAL. Recently, attention has focused on PALs that adopt the phased array technique,³ which means that the velocity profile for the ultrasound follows a tailored amplitude and phase distribution. One typical application is a steerable PAL, which can deliver directional audio beams in a desired direction without physically rotating the PAL.^{3–7} Such a phased array PAL has been successfully used in active noise control,³ sound reproduction systems,⁸ immersive three-dimensional (3D) audio,⁹ and related areas.^{4,10} However, the existing models suitable for predicting the performance of a phased array PAL are not only limited for far field calculations but also the simplifying assumptions and approximations deteriorate their accuracy.^{11,12}

Because this generation is a nonlinear process, the total audio sound generated by a phased array PAL is not simply the superposition of the audio sound radiated by each PAL element. Therefore, one must start from the governing equations to obtain the accurate predictions. When a PAL radiates two intensive ultrasonic waves at different frequencies, a secondary wave containing the difference-frequency wave (the audio wave in air) is generated as a result of a second-order nonlinearity.² This process can be modelled using a second-order nonlinear wave equation if the cubic and higher order terms are neglected.^{13–15} After neglecting the Lagrangian density characterizing the local effects, the equation can be further simplified to give the Westervelt equation, which is often used instead because it is easier to solve.^{14,15} It has also been demonstrated that the predictions obtained using the Westervelt equation are accurate enough except for the observation points close to the radiation surface of the PAL.^{14,15}

After using the successive method,¹⁶ the quasilinear solution of the audio sound based on the Westervelt equation can be seen as the radiation from a virtual volume source with the source density proportional to the product of the ultrasound pressure.^{17,18} The expression of the solution is, therefore, a threefold integral over the 3D space. The ultrasound pressure at the virtual source point is then obtained using the twofold Rayleigh integral as the ultrasound beams can be modelled as the radiation from a baffled rigid source. The accurate calculation of the audio sound generated by a PAL then requires a numerical evaluation of a fivefold integral expression.^{17–19}

^{a)}ORCID: 0000-0002-9972-8004.

^{b)}ORCID: 0000-0002-3520-1377.

^{c)}ORCID: 0000-0002-2949-5364.

^{d)}Electronic mail: hszou@nju.edu.cn

The direct numerical integration of this fivefold integral expression is known to be very time-consuming, and some approximations and assumptions are usually made to simplify the calculations. The paraxial model has been widely used and this assumes paraxial approximations for both the audio and ultrasound beams so that a Gaussian beam expansion (GBE) can be used to simplify the integral into a summation of the contribution from a set of Gaussian sources.^{17,20,21} The prediction accuracy of the paraxial model is the same as that of the well-known Khokhlov-Zabolotskaya-Kuznetsov (KZK) equation,^{17,22} but the results are accurate only inside the paraxial region.^{17,22} Furthermore, the prediction of the paraxial model is also known to be inaccurate at low frequencies. One way to overcome this problem is to assume the paraxial approximation only for ultrasound, which is termed the non-paraxial model.^{17,19,23,24} However, because the paraxial approximation for the ultrasound is retained in the non-paraxial model, it is still inaccurate when the sound beams of a phased array PAL are steered to a larger angle. Recently, a spherical expansion has been developed to give a rigorous simplification of the fivefold integral into a threefold series consisting of uncoupled radial and angular components,^{15,18} which converges more than 100 times faster. Although no paraxial approximations are assumed in the spherical expansion, it can only be applied to the PAL with a velocity profile that is axisymmetric about the radiation axis.

To avoid the heavy computation load, many models have been proposed to obtain much simpler expressions in the far field.⁸ The first closed-form expression for audio beam directivity was proposed in Westervelt's seminal work, and this is usually termed the Westervelt directivity.² However, large differences between the predictions obtained using Westervelt's directivity and experimental measurements have been reported,⁸ and this is thought to be because the ultrasound beams are assumed to be collimated and all nonlinear interactions happen only over a limited distance. Many attempts have been made to improve the accuracy of the directivity predictions such as considering the directivity of ultrasound beams.^{6,25-27}

The most accurate approach to date for the far field is to employ the convolution of the ultrasonic wave directivities and Westervelt's directivity.^{11,12} An arbitrary directivity for the ultrasound can then be set in the convolution model to calculate the audio sound directivity, and reported experimental results have demonstrated that it outperforms other existing models in the far field for a steerable PAL.^{8,11} However, the ultrasound beams are assumed to be exponentially attenuated in each direction, which is not true in reality because of the complexity of the ultrasound beams in the near field, where the majority of the nonlinear interactions take place. Furthermore, the far field is found to be more than 10 m away from a PAL when its size is larger than 0.04 m,^{15,28} which is too far when compared to real applications. Therefore, differences between the predictions and measurements continue to be observed, even for the sound pressure 4 m away from the PAL.¹¹

The rectangular phased array PAL is the most common PAL in industrial applications. Due to the poor convergence

of the Rayleigh integral, it is hard to directly calculate the radiation from a rectangular source. When one dimension of the radiation surface of a piston source is much larger than the wavelength, the radiated sound field can be approximately modelled as the radiation from the infinitely long strips.^{29,30} After using the integral expression of the Hankel function (also known as the two-dimensional Green's function), the twofold Rayleigh integral can be simplified into a onefold Rayleigh integral. Based on such a model, the sound field radiated by a conventional loudspeaker has been extensively studied.²⁹ A cylindrical expansion for a conventional loudspeaker was recently proposed based on the translational addition theorem for Hankel functions.³⁰ This can be regarded as the two-dimensional version of the spherical expansion for the sound field radiated by a circular piston source.^{18,31,32} The cylindrical expansion converges quickly because no integral with a highly oscillatory integrand is required to calculate. In addition, the radial and angular coordinates are uncoupled (separated) so that they can be computed quickly for many observation points. Another advantage is that an arbitrary velocity profile can be set for the radiation surface so that it can be used to model a phased array. However, the cylindrical expansion for the audio sound generated by a PAL has not been developed yet.

In this paper, a cylindrical expansion for the ultrasound is introduced by modelling the radiating surface as a baffled phased ultrasonic source with one infinitely long dimension. Next, the expansion for the audio sound is developed in cylindrical coordinates using a quasilinear solution of the Westervelt equation without further approximations. The numerical results for the audio sound are presented for a steerable PAL with several typical excitation velocity profiles. The accuracy of the convolution model is then compared against this proposed model, and predictions from both of the models are compared against the experimental results reported in Ref. 11.

II. THEORY

Figure 1 shows the sketch of a baffled phased array PAL radiating ultrasound in the free field. The rectangular (x, y, z) and cylindrical (ρ, ϕ, z) coordinate systems are established with their origin, O , at the center of the PAL and the positive y axis pointing to the radiation direction, where ρ and ϕ are the radial and polar angle coordinates, respectively. It is assumed that the dimension of the PAL along the z axis is infinitely long such that only the sound field on the plane xOy needs to be considered. The length of the phased array PAL along the x axis is $2a$.

To predict the sound fields generated by a PAL using the phased array technique, the boundary condition for the ultrasound is assumed on $y = 0$ to be

$$u_t(x) = u(x, k_1)e^{-i\omega_1 t} + u(x, k_2)e^{-i\omega_2 t}, \quad -a \leq x \leq a, \quad (1)$$

where $u(x, k_i)$ is an arbitrary complex velocity profile for the ultrasound at the wavenumber $k_i = \omega_i/c_0 + i\alpha_i$, $\omega_i = 2\pi f_i$ is the angular frequency, f_i is the i th ultrasonic frequency, $i = 1$

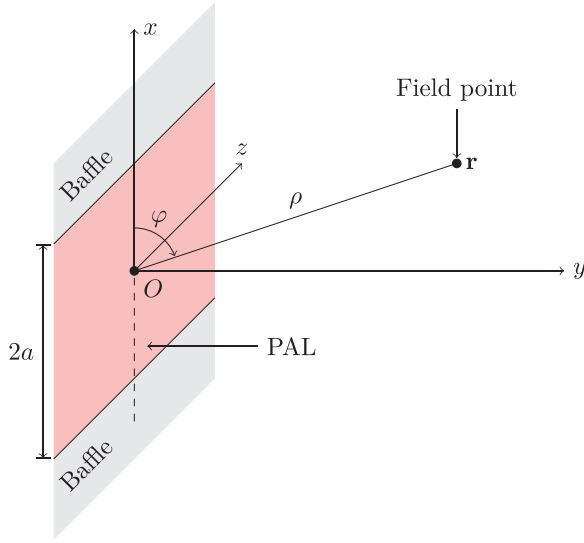


FIG. 1. (Color online) Sketch of a phased array PAL and the geometrical description of the rectangular and cylindrical coordinate systems.

and $2, f_1 > f_2$, α_i is the sound attenuation coefficient for the i th ultrasonic wave, c_0 is the linear sound speed, i is the imaginary unit, and t is the time.

A. Westervelt equation and quasilinear solution

The Westervelt equation is given as^{14,15}

$$\nabla^2 p - \frac{1}{c_0^2} \frac{\partial^2 p}{\partial t^2} + \frac{\delta}{c_0^2} \nabla^2 \frac{\partial p}{\partial t} = -\frac{\beta}{\rho_0 c_0^4} \frac{\partial^2 p^2}{\partial t^2}, \quad (2)$$

where ρ_0 is the ambient density, p is the sound pressure, $\beta = 1.2$ is the nonlinear coefficient in air, and δ is the sound diffusivity parameter. It has been demonstrated that the Westervelt equation can correctly describe the cumulative nonlinear interactions of ultrasound to the second order, which is accurate enough for many applications.^{14,15,33}

By using the successive method, the quasilinear solution of the audio sound pressure is expressed as a volume integral over the whole space,^{17,18}

$$p_a(\mathbf{r}) = -i\rho_0\omega_a \int_{-\infty}^{\infty} \int_{-\infty}^{\infty} \int_{-\infty}^{\infty} q(\mathbf{r}_v) \frac{e^{ik_a|\mathbf{r}-\mathbf{r}_v|}}{4\pi|\mathbf{r}-\mathbf{r}_v|} dx_v dy_v dz_v, \quad (3)$$

where $k_a = \omega_a/c_0 + i\alpha_a$ is the wave number for the audio sound at the angular frequency of ω_a , $\omega_a = 2\pi f_a$, α_a is the sound attenuation coefficient at the audio frequency of f_a , $f_a = f_1 - f_2$, $|\mathbf{r} - \mathbf{r}_v| = \sqrt{(x-x_v)^2 + (y-y_v)^2 + (z-z_v)^2}$ is the distance between the point $\mathbf{r} = (x, y, z)$ and the virtual source point or its image $\mathbf{r}_v = (x_v, y_v, z_v)$, and the source density is

$$q(\mathbf{r}) = \frac{\beta\omega_a}{i\rho_0^2 c_0^4} p_1(\mathbf{r}) p_2^*(\mathbf{r}), \quad (4)$$

where the superscript “*” represents the complex conjugate. It is noted in Eq. (3) that the integration interval from 0 to ∞ over y_v represents the contribution from the original

virtual source in front of the PAL, and the integration interval from $-\infty$ to 0 over y_v is the contribution from the image of virtual sources with respect to the baffle at $y = 0$.

The ultrasound pressure can be obtained by the Rayleigh integral as

$$p_i(\mathbf{r}) = -2i\rho_0\omega_i \int_{-a}^a \int_{-\infty}^{\infty} \frac{e^{ik_i|\mathbf{r}-\mathbf{r}_s|}}{4\pi|\mathbf{r}-\mathbf{r}_s|} u(x_s, k_i) dz_s dx_s, \quad (5)$$

$i = 1, 2,$

where $|\mathbf{r} - \mathbf{r}_s| = \sqrt{(x-x_s)^2 + y^2 + (z-z_s)^2}$ is the distance between the point \mathbf{r} and the source point $\mathbf{r}_s = (x_s, 0, z_s)$ on the PAL surface.

After substituting Eqs. (4) and (5) into Eq. (3), a five-fold integral must be calculated numerically to obtain the audio sound, and this process is known to be very time-consuming.^{15,17,18} Many methods have been proposed to simplify the calculation of the ultrasound in Eq. (5), subject to the paraxial approximation.¹⁷ However, the paraxial approximation is inaccurate when the sound beams of a phased array PAL are steered to a larger angle. Recently, a spherical expansion method was proposed, which is at least 15 times faster than a GBE without the paraxial approximation.^{15,18} Unfortunately, it can only be applied to the PAL with a velocity profile that is axisymmetric about the radiation axis.

B. Convolution model in the far field

In the inverse-law far field, where the audio sound pressure is inversely proportional to the propagation distance, the expression of the audio sound can be further simplified.¹⁵ The directivity for the audio sound, $D_a(\theta)$ is defined as $|p_a(\theta)/p_a(\theta=0)|$, where θ is defined as the angle between the field point and the radiation axis ($\varphi = \pi/2$ in Fig. 1) so that $\theta = |\varphi - \pi/2|$. The convolution method assumes that the field point is in the inverse-law far field, where a good agreement between the predictions and measurements has been shown using this method.^{11,12} This method is, therefore, used for the purpose of comparison against the proposed alternative approach and is briefly summarized here.

The directivity of the audio sound is obtained by the convolution model as^{11,12}

$$D_a(\theta) = [D_1(\theta)D_2(\theta)] * D_w(\theta), \quad (6)$$

where $D_1(\theta)$ and $D_2(\theta)$ are the directivities of the ultrasound, “*” denotes the linear convolution operation, and $D_w(\theta)$ is Westervelt’s directivity,^{11,12}

$$D_w(\theta) = \frac{1}{\sqrt{1 + k_a^2 \tan^4 \theta / (\alpha_1 + \alpha_2)^2}}. \quad (7)$$

The ultrasound in the convolution model is assumed to be exponentially attenuated in each direction, which is not

true in reality because of the complexity of the ultrasound beams in the near field of the transducers. Therefore, some discrepancies are observed between the measurements and predictions in Ref. 11. To address this, cylindrical expansions of both the ultrasound and audio sound are derived in Secs. II C and II D, respectively, and the predictions are compared against the convolution method in Sec. IV.

C. Cylindrical expansion of ultrasound

By evaluating the Rayleigh integral with respect to z_s and using the integral definition for a Hankel function of order 0, $H_0(\cdot)$, Eq. (5) can be simplified as^{30,34}

$$p_i(\mathbf{r}) = \frac{\rho_0 \omega_i}{2} \int_{-a}^a H_0(k_i |\mathbf{r} - \mathbf{r}_s|) u(x_s, k_i) dx_s. \quad (8)$$

To express Eq. (8) as a cylindrical expansion, the translational addition theorem for the Hankel function is introduced such that^{30,34}

$$H_0(k_i |\mathbf{r} - \mathbf{r}_s|) = \sum_{n=-\infty}^{\infty} J_n(k_i \rho_{s,<}) H_n(k_i \rho_{s,>}) e^{in(\varphi - \varphi_s)}, \quad (9)$$

where $J_n(\cdot)$ and $H_n(\cdot)$ are the Bessel and Hankel functions of order n , respectively, $\rho_{s,<}$ represents the lesser of ρ and ρ_s , and $\rho_{s,>}$ the greater of the two. For the source point on the positive x axis, $x_s = \rho_s$ and $\varphi_s = 0$; for the source point on the negative x axis, $x_s = -\rho_s$ and $\varphi_s = \pi$. Substituting Eq. (9) into Eq. (8) yields

$$p_i(\mathbf{r}) = \frac{\rho_0 c_0}{2} \sum_{n=-\infty}^{\infty} R_n(\rho, k_i) e^{in\varphi}, \quad (10)$$

where the radial component for the ultrasound is

$$R_n(\rho, k_i) = \int_0^a J_n(k_i \rho_{s,<}) H_n(k_i \rho_{s,>}) u(\rho_s, k_i) k_i d\rho_s + e^{-in\pi} \int_0^a J_n(k_i \rho_{s,<}) H_n(k_i \rho_{s,>}) u(-\rho_s, k_i) k_i d\rho_s. \quad (11)$$

By introducing the substitution

$$u_n(\rho_s, k_i) = u(\rho_s, k_i) + (-1)^n u(-\rho_s, k_i), \quad (12)$$

Eq. (11) is rewritten in a more compact form,

$$R_n(\rho, k_i) = \int_0^a J_n(k_i \rho_{s,<}) H_n(k_i \rho_{s,>}) u_n(\rho_s, k_i) k_i d\rho_s. \quad (13)$$

Compared to the original twofold integral in Eq. (5), the cylindrical expansion in Eq. (10) is more computationally efficient for three reasons. First, a twofold integral with a highly oscillatory integrand is required to evaluate in Eq. (5). Second, the radial and angular coordinates, ρ and φ , are uncoupled (separated) in Eq. (10) such that the radial and angular components can be calculated separately to obtain

the sound pressure for many field points. Finally, for the most field points when $\rho > a$, $J_n(k_i \rho_{s,<}) H_n(k_i \rho_{s,>})$ becomes $J_n(k_i \rho_s) H_n(k_i \rho)$ in Eq. (13), and the integral needs to be calculated only one time for each order n at the different field points. In addition, the integral in Eq. (13) can be further simplified to a series by using the power expansion of the Bessel function.³⁰

To obtain the directivity of the ultrasound used in the convolution method in Eq. (6), the radial component given by Eq. (13) can be simplified using the limiting forms of the Hankel functions for large arguments; see Eq. (5.1.17) in Ref. 35, such that

$$R_n(\rho \rightarrow \infty, k_i) = \sqrt{\frac{2}{\pi k_i \rho}} \frac{e^{ik_i \rho}}{i^{n+1/2}} \int_0^a J_n(k_i \rho_s) u_n(\rho_s, k_i) k_i d\rho_s, \quad (14)$$

which is valid in the far field.

D. Cylindrical expansion of audio sound

Substituting Eq. (10) into the source density of the audio sound given by Eq. (4), one obtains the cylindrical expansion of Eq. (4) as

$$q(\mathbf{r}) = \frac{\beta \omega_a}{4ic_0^2} \sum_{m=-\infty}^{\infty} \sum_{n=-\infty}^{\infty} R_m(\rho, k_1) R_n^*(\rho, k_2) e^{i(m-n)\varphi}. \quad (15)$$

Similar to Eq. (8), the audio sound pressure in Eq. (3) can be obtained as

$$p_a(\mathbf{r}) = \frac{\rho_0 \omega_a}{4} \int_0^{2\pi} \int_0^\infty q(\mathbf{r}_v) H_0(k_a |\mathbf{r} - \mathbf{r}_v|) \rho_v d\rho_v d\varphi_v. \quad (16)$$

Substituting Eqs. (9) and (15) into Eq. (16), one obtains

$$p_a(\mathbf{r}) = \frac{\beta \pi \rho_0}{8i} \sum_{m=-\infty}^{\infty} \sum_{n=-\infty}^{\infty} \sum_{l=-\infty}^{\infty} e^{il\varphi} \left[\frac{1}{2\pi} \int_0^{2\pi} e^{i(m-n-l)\varphi_v} d\varphi_v \right] \times \int_0^\infty R_m(\rho_v, k_1) R_n^*(\rho_v, k_2) J_l(k_a \rho_{v,<}) \times H_l(k_a \rho_{v,>}) k_a^2 \rho_v d\rho_v, \quad (17)$$

where $\rho_{v,<}$ represents the lesser of ρ and ρ_v , and $\rho_{v,>}$ is the greater of the two. Only the terms when $l = m - n$ are left in Eq. (17) because

$$\frac{1}{2\pi} \int_0^{2\pi} e^{i(m-n-l)\varphi_v} d\varphi_v = \begin{cases} 1, & l = m - n, \\ 0, & l \neq m - n. \end{cases} \quad (18)$$

The audio sound pressure may then be reduced to a cylindrical expansion, which yields

$$p_a(\mathbf{r}) = \frac{\beta \pi \rho_0}{8i} \sum_{m=-\infty}^{\infty} \sum_{n=-\infty}^{\infty} \chi_{mn}(\rho) e^{i(m-n)\varphi}, \quad (19)$$

where the radial component for the audio sound is expressed as

$$\chi_{mn}(\rho) = \int_0^\infty R_m(\rho_v, k_1) R_n^*(\rho_v, k_2) J_{m-n}(k_a \rho_{v,<}) \times H_{m-n}(k_a \rho_{v,>}) k_a^2 \rho_v d\rho_v. \quad (20)$$

In the far field, Eq. (20) has the limiting form

$$\chi_{mn}(\rho \rightarrow \infty) = \sqrt{\frac{2}{\pi k_a \rho}} e^{ik_a \rho} \times \int_0^\infty R_m(\rho_v, k_1) R_n^*(\rho_v, k_2) \times J_{m-n}(k_a \rho_v) k_a^2 \rho_v d\rho_v. \quad (21)$$

As the main result of this paper, the cylindrical expansion of the audio sound given by Eq. (19) consists of a series of two summations with the uncoupled radial and angular components, thus, it can be calculated quickly for many field points. It can be seen as a two-dimensional version of the spherical expansion as developed in Refs. 15 and 18, which is a series of triple summations. It has been demonstrated that the calculation of the spherical expansion is more than 100 times faster than the direct integration of the fivefold integral given by Eq. (3) after the substitution of Eqs. (4) and (5). The cylindrical expansion is simpler than the spherical expansion; hence, the computational efficiency is further improved. In addition, the arbitrary excitation velocity profiles, $u(x, k_i)$, can be assumed for the ultrasound source in Eq. (13), and so it can be used to model a phased array PAL.

E. Velocity profiles for a steerable PAL

In this paper, a steerable PAL is used as an example of the proposed cylindrical expansion, which aims to steer the audio beam in a desired direction. The phased array technique assumes that an excitation of an array of PALs consists of an amplitude and a phase at each PAL element.⁸

For the ideal configuration, when the size of the PAL element is infinitely small, a continuous velocity profile can be assumed as

$$u(x, k_i) = u_0 e^{ik_i x \cos \varphi_0}, \quad (22)$$

where u_0 is a constant with the units of m/s, and φ_0 is the steering angle such that $0 \leq \varphi_0 \leq \pi$.

For the non-ideal configuration, when the PAL element has a finite size of a_0 (also known as the sub-array size), the phase distribution on the radiation surface of each element must be uniform. Therefore, the discrete profile is given by a relation to the continuous profile as

$$u_{\text{dis}}(x, k_i) = u \left(\left(\left\lfloor \frac{x}{a_0} \right\rfloor + \frac{1}{2} \right) a_0, k_i \right). \quad (23)$$

In real applications, the separation between the centers of the adjacent PAL elements may be larger than their size

so as to give a blank region on the rigid baffle (also known as the array kerf).¹¹ This can be modelled by multiplying the profiles in Eqs. (22) and (23) with a weighting function such that the weight is zero in the blank region, which reads

$$A(x) = \begin{cases} 1, & -\frac{a_1}{2} \leq x - \left(\left\lfloor \frac{x}{a_0} \right\rfloor + \frac{1}{2} \right) a_0 \leq \frac{a_1}{2}, \\ 0 & \text{otherwise,} \end{cases} \quad (24)$$

where a_1 is the distance between the centers of the adjacent PAL elements.

To better understand the continuous and discrete velocity profiles for a steerable PAL, Fig. 2 shows a comparison between them for the amplitudes and phases. The parameters used are the same as those in Fig. 8 of Ref. 11: the PAL is steered at 70° with a carrier frequency of 40 kHz, the phased array PAL size is $2a = 0.1$ m, the size of each PAL element is $a_0 = 0.01$ m, and the separation of the centers of the adjacent elements is $a_1 = 0.0125$ m.

III. NUMERICAL ALGORITHMS

The cylindrical expansion of the audio sound in Eq. (19) is a series which must be truncated to obtain the numerical results. The truncation limit is set to 70 for both m and n in the following simulations, which deliver an error of less than 0.1 dB for the parameters used in this paper. The one-fold integrals in Eqs. (13) and (20) are calculated using the classical Gauss-Legendre quadrature method, although the computational efficiency can be further improved using the series expression and complex plane method.^{18,30} The sound attenuation coefficients for both the ultrasound and audio

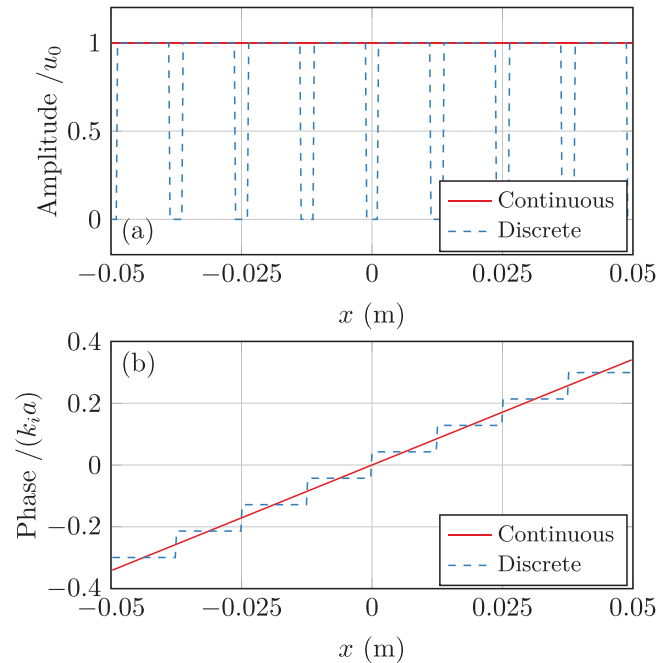


FIG. 2. (Color online) The comparison of the continuous and discrete velocity profile for the ultrasound. The (a) normalized amplitude distribution and (b) normalized phase distribution are shown.

sound are estimated according to ISO 9613.³⁶ The directivities of the ultrasound used in Eq. (6) of the convolution model are obtained using the cylindrical expansion in Eq. (10) with the limiting form of the radial component at large arguments in Eq. (14).

It is found in the simulations that the calculation of the Bessel functions overflow or underflow when the argument is much smaller than the order. Therefore, the normalized Bessel and Hankel functions are used in this paper and defined as

$$\bar{J}_n(w) = n! \left(\frac{2}{w} \right)^n J_n(w), \quad (25)$$

$$\bar{H}_n(w) = \frac{i\pi}{n!} \left(\frac{w}{2} \right)^n H_n(w), \quad (26)$$

where “!” represents the factorial. Using these definitions, the normalized Bessel and Hankel functions have the limiting behavior when $|w| \rightarrow 0$ as

$$\bar{J}_n(w) \rightarrow 1, \quad n\bar{H}_n(w) \rightarrow 1. \quad (27)$$

The following relation, required in Eqs. (13) and (20), is then obtained as

$$J_n(w_1)H_n(w_2) = \frac{1}{i\pi} \left(\frac{w_1}{w_2} \right)^n \bar{J}_n(w_1)\bar{H}_n(w_2). \quad (28)$$

Equations (25) and (26) are similar to the normalization technique used to solve the overflow problem in the

calculation of the spherical Bessel functions.^{18,37} The recurrence relations [see Eq. (5.1.21) in Ref. 35] yield

$$\bar{J}_{n+1}(w) = \frac{1}{4n(n+1)} [\bar{J}_n(w) - \bar{J}_{n-1}(w)], \quad (29)$$

$$\bar{H}_{n+1}(w) = \frac{n}{n+1} \bar{H}_n(w) - \frac{w^2}{4n(n+1)} \bar{H}_{n-1}(w). \quad (30)$$

The numerical results can then be obtained using the backward and forward recurrence relations given by Eqs. (29) and (30), respectively.

IV. RESULTS

To compare against the experimental data in the literature, the parameters are set to be the same as those in Ref. 11. The center frequency of the ultrasound is 40 kHz, and all of the sound pressure levels (SPLs) in the following simulations are normalized with a maximum of 0 dB to aid the comparison. The medium is assumed to be air and the temperature is set as 20 °C.

A. Conventional PAL with a uniform excitation

In this subsection, a continuous uniform velocity profile is assumed as this best represents a conventional PAL. Figure 3 shows the audio sound fields generated by a conventional PAL with a size of $2a = 0.08$ m at 500 Hz, 1 kHz, 2 kHz, and 4 kHz. The Rayleigh distance is about 0.6 m at 40 kHz. The

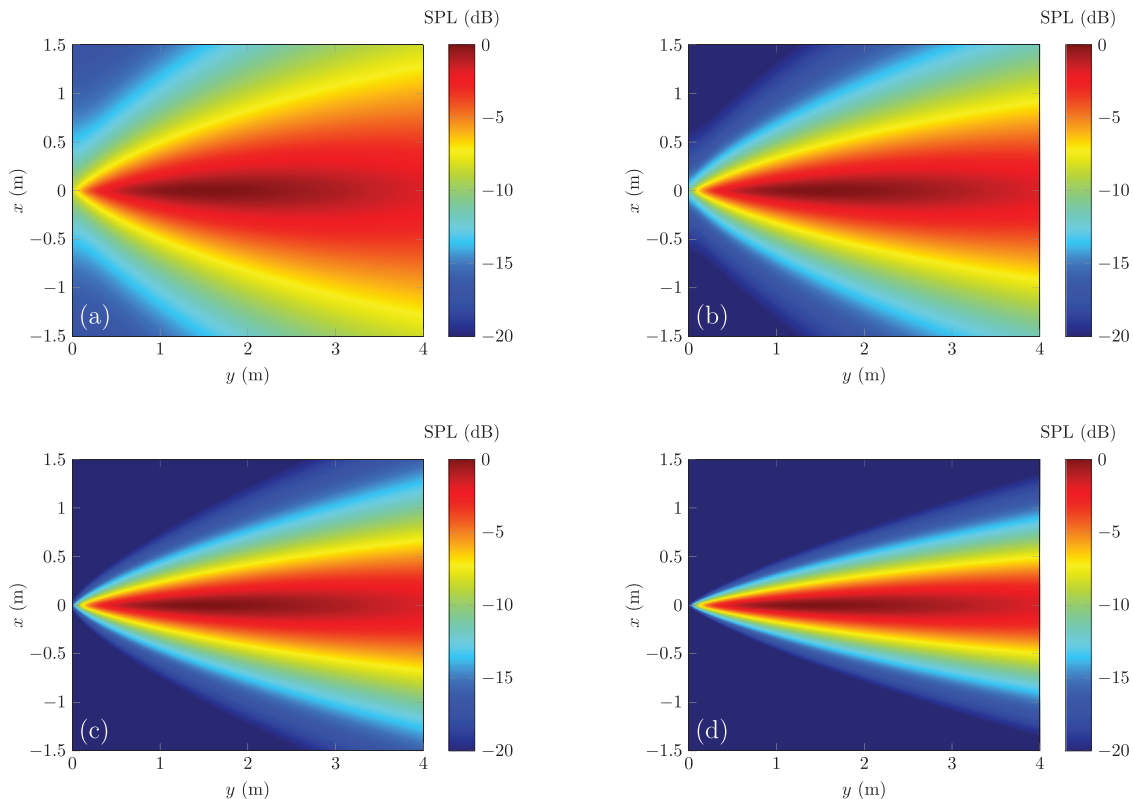


FIG. 3. (Color online) The audio sound fields generated by a conventional PAL with a uniform profile and a size of 0.08 m at (a) 500 Hz, (b) 1 kHz, (c) 2 kHz, and (d) 4 kHz.

results are obtained using the proposed cylindrical expansion. It is observed that the mainlobe of the generated audio beam is on the radiation axis so that $\varphi_0 = 90^\circ$, and the beam becomes more focused as the frequency increases.

The directivity of the audio sound beam in the far field at different angles and frequencies is shown in Fig. 4 using the far field solution of the cylindrical expansion [Eqs. (19) and (21)]. Because the sound pressure was measured at 4 m away from the PAL in Ref. 11, the results at a radial distance of 4 m are calculated using the cylindrical expansion [Eqs. (19) and (20)], and these are also presented in Fig. 4. It is interesting to note that the difference between these two curves is large at most angles. For example, the difference at 70° is 3.3 dB, 2.7 dB, 1.7 dB, and 2.1 dB at 500 Hz, 1 kHz, 2 kHz, and 4 kHz, respectively. It indicates that the far field solution is inaccurate for predicting the audio sound at 4 m away from the PAL. To obtain the accurate predictions using the far field solution, the observation point should be far away from the virtual source of the audio sound rather than the Rayleigh distance. As demonstrated by Zhong *et al.*,¹⁵ an empirical formula of $4/\alpha_u$ can be used to estimate the far field transition distance, where α_u is the ultrasound attenuation coefficient at the average ultrasound frequency. The far field transition distance is about 32 m at 40 kHz, which is seen to be much larger than the Rayleigh distance of 4 m. Therefore, only those results at a radial distance of 4 m obtained using the cylindrical expansion are presented in Figs. 6 and 8.

The directivity of the audio sound beam in the far field can also be obtained using Eq. (6) of the convolution model, thus, the results calculated using this approach are presented in Fig. 4 for comparison. It can be seen in Fig. 4 that the SPL values calculated using the convolution model are slightly larger than those of the cylindrical expansion at a radius of 4 m for angles around 90° and smaller at other angles. For example, in Fig. 4(d), the SPL obtained at 4 m using the convolution model for a frequency of 4 kHz is 0.8 dB larger and 1.6 dB smaller than that obtained with a cylindrical expansion at 94.1° and 102.1° , respectively. This difference becomes larger as the frequency decreases, indicating that the accuracy using the convolution model deteriorates at low frequencies.

The measured audio sound directivities at 4 kHz are available from Fig. 4 of Ref. 11 and they are presented in Fig. 4(d). The ultrasound directivities are required to obtain the audio sound directivity in the convolution model as shown in Eq. (6). They are predicted using Eqs. (10) and (14) in this paper but obtained by the measurement in Ref. 11. Therefore, the results obtained using the convolution model in Ref. 11 can be different, and they are also presented in Fig. 4(d) for comparison. It can be seen in Fig. 4(d) that the SPL values obtained with the cylindrical expansion at 4 m provide better agreement with the measurement when compared to the convolution model for angles larger than 85° . For example, the difference between the measurement and the value obtained using the cylindrical expansion

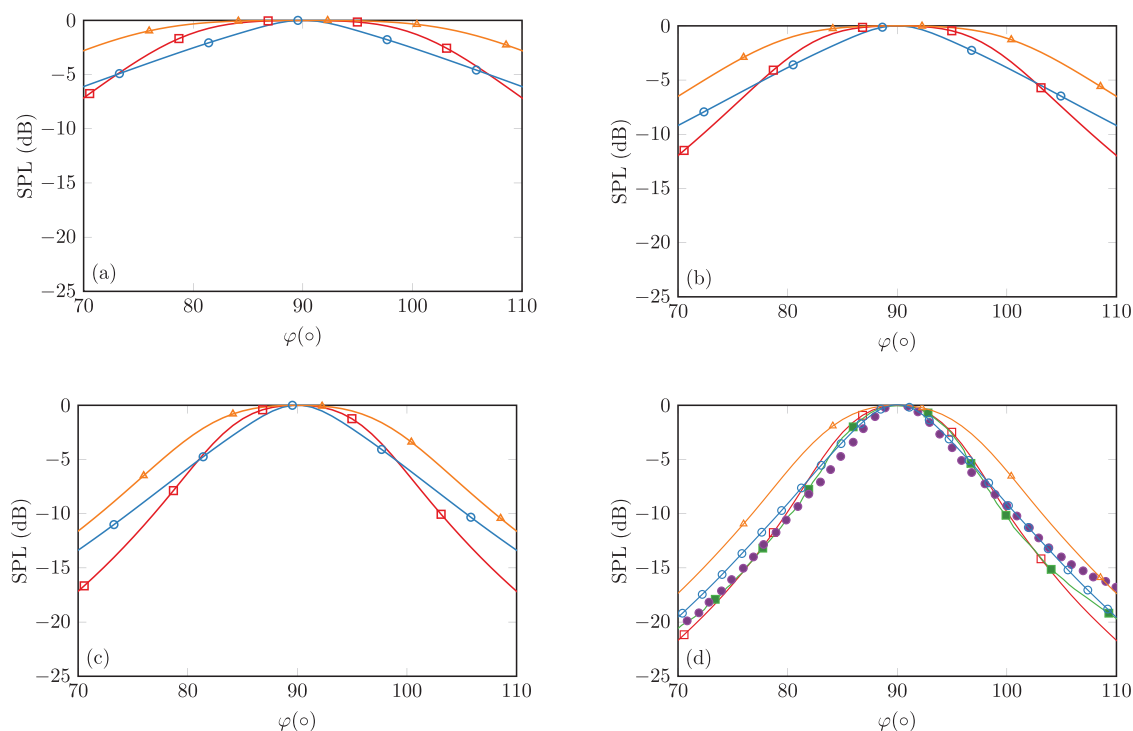


FIG. 4. (Color online) The audio SPL generated by a conventional PAL with a uniform profile and a size of 0.08 m, calculated using the convolution method and cylindrical expansion at (a) 500 Hz, (b) 1 kHz, (c) 2 kHz, and (d) 4 kHz. Red hollow square, convolution model; blue hollow circle, cylindrical expansion at 4 m; orange triangle, cylindrical expansion in the far field; green solid square, convolution method from Ref. 11; and purple solid circle, measurement from Ref. 11.

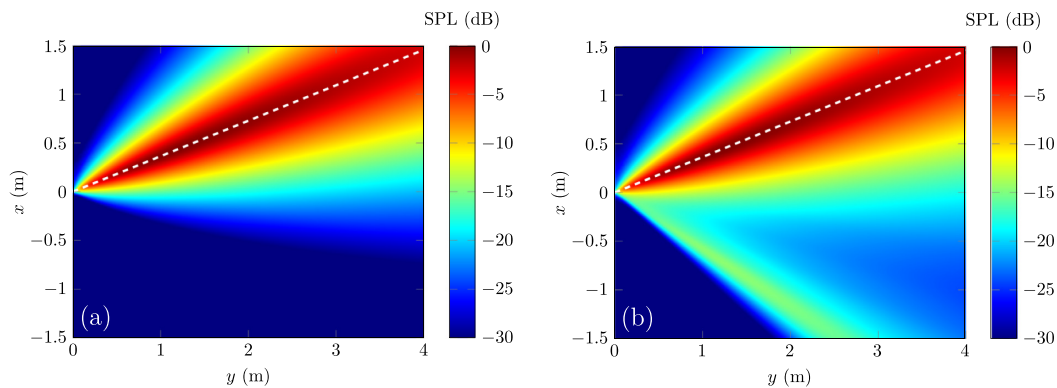


FIG. 5. (Color online) The audio sound fields at 4 kHz generated by a steerable PAL with a steering angle of 70° (denoted by dashed lines), a size of 0.08 m, and a (a) continuous or (b) discrete profile with a PAL element size of 0.01 m.

is only 0.5 dB at 94.8° , whereas it increases to 1.5 dB when compared to the convolution model.

B. Steerable PAL generating one beam

The steerable PAL with a steering angle of 70° used in Sec. III C of Ref. 11 is considered in this subsection. Figure 5 shows the audio sound fields at 4 kHz, generated by a steerable PAL with a continuous or discrete profile, where the size of the phased array PAL is $2a = 0.08$ m, and the size of the PAL element is $a_0 = 0.01$ m. Comparing Fig. 5(a) to Fig. 3(d) demonstrates the ability of a phased array PAL to steer the audio beam in a desired direction. When the velocity profile is discrete (which is usually limited by the size of the real ultrasonic transducers), a sidelobe would occur around 120° as shown in Fig. 5(b). This is known as the spatial aliasing phenomenon, arising from the fact that the size of the PAL element (0.01 m) is greater than half of the wavelength of the ultrasound (0.0086 m at 40 kHz).⁶

Figure 6 compares the audio SPL at different angles using the convolution model and the cylindrical expansion at a radial distance of 4 m. The measurement data and results obtained using the convolution model and measured ultrasound directivities in Ref. 11 are also presented for comparison. It can be found both models are able to predict similar results around the mainlobe at 70° . The sidelobe is 115° for the data in Ref. 11, whereas it is 120° for the predictions in this paper. The reason may arise from the measurement error, imperfect positioning of the phased array, and so on. The experimental result at the sidelobe (115°) in Ref. 11 is 3.1 dB below the prediction from the convolution model, which can be more accurately predicted by the cylindrical expansion as a decrement (3.0 dB) can be observed at the sidelobe (120°). It indicates that the cylindrical expansion is more appropriate for the prediction of a steerable PAL with a discrete profile. Furthermore, the cylindrical expansion can predict the details of the sound field in the near field as shown in Fig. 5.

C. Steerable PAL generating dual beams

The generation of an unwanted sidelobe when using a discrete velocity profile for a steerable PAL was shown in

Sec. IV B. However, this effect can be used to generate dual audio beams; see Ref. 6 for more details. For example, Fig. 7 shows a 4 kHz dual audio beam at 70° and 110° using the parameters in Fig. 8 of Ref. 11, and this was achieved by steering the ultrasound beams to 69° and 71° at 38 and 42 kHz, respectively. The size of the phased array PAL is $2a = 0.1$ m, the size of the PAL elements is $a_0 = 0.01$ m, their center separation is $a_1 = 0.0125$ m, and the velocity profile is illustrated in Fig. 2. The details of the audio sound in the near field shown in Fig. 7 demonstrate that this method can successfully generate dual beams with an acceptable acoustic contrast in the full field.

The audio SPL at different angles, obtained using the proposed cylindrical expansion and convolution model, is compared in Fig. 8. The measurement data and results obtained using the convolution model and ultrasound directivities in Ref. 11 are also presented. As shown in Fig. 8, it is clear the cylindrical expansion provides a much better agreement with the measurement data. At the angles between the two lobes, the SPL values obtained using the convolution model are lower than those found using the cylindrical expansion. The difference between the two is a maximum of

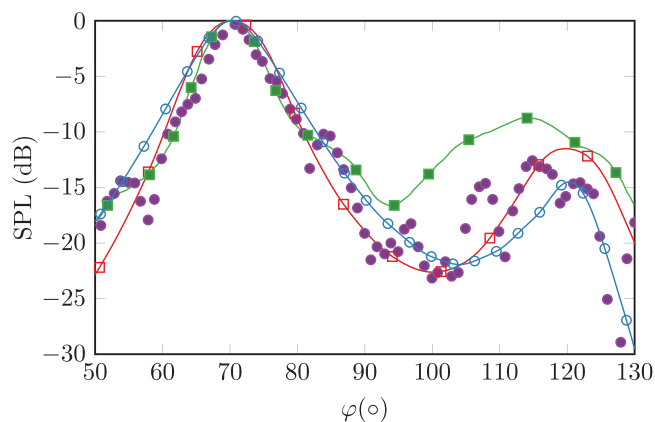


FIG. 6. (Color online) The audio SPL at 4 kHz at different angles generated by a steerable PAL with a steering angle of 70° , a size of 0.08 m, and a discrete profile with a PAL element size of 0.01 m. Red hollow square, convolution model; blue hollow circle, cylindrical expansion at 4 m; green solid square, convolution model from Ref. 11; and purple solid circle, measurement from Ref. 11.

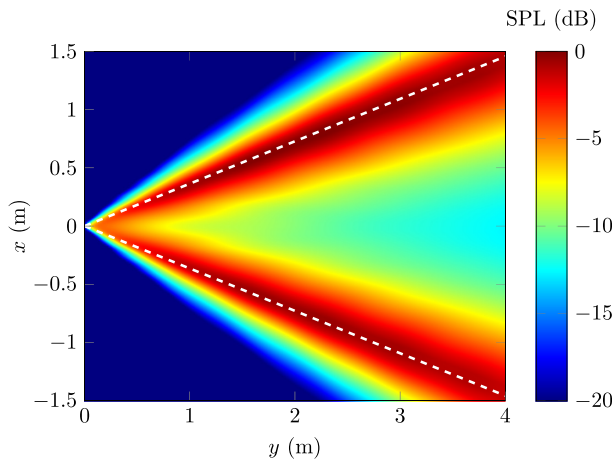


FIG. 7. (Color online) The audio sound fields at 4 kHz generated by a steerable PAL generating dual beams at 70° and 110° (denoted by dashed lines), where the size of the phased array PAL is 0.1 m, the size of PAL elements is 0.01 m, and their center separation is 0.0125 m.

5.8 dB at 90° . The nonlinear interactions between the ultrasonic waves in the near field become more complex in this case when compared to a conventional PAL with a uniform excitation. These interactions cannot be captured in the convolution model because only the far field directivity for the ultrasound is used. The prediction accuracy is, therefore, deteriorated significantly in this case. However, no simplifications for the ultrasound are made in the cylindrical expansion, hence, it provides a more accurate solution.

V. CONCLUSIONS

In this paper, a cylindrical expansion for the radiation from infinitely long strips was reviewed. The cylindrical expansion was then extended for the audio sound generated by a PAL after adopting the phased array technique based on a quasilinear solution of the Westervelt equation. The expansion is a series of twofold summations with uncoupled angular and radial components in the cylindrical coordinate system. The angular

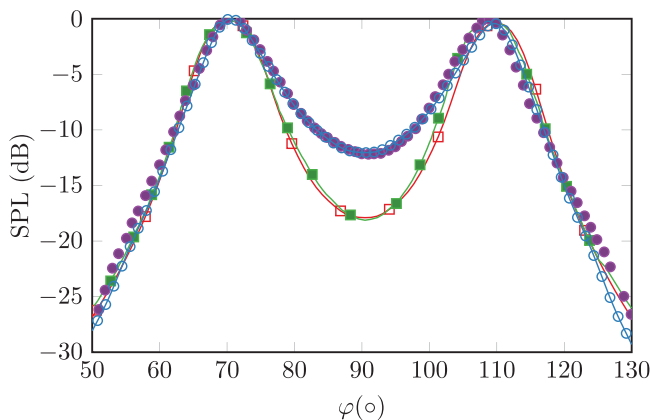


FIG. 8. (Color online) The audio SPL at 4 kHz at different angles generated by a steerable PAL generating dual beams at 70° and 110° , where the size of the phased array PAL is 0.1 m, the size of PAL elements is 0.01 m, and their center separation is 0.0125 m. Red hollow square, convolution model; blue hollow circle, cylindrical expansion at 4 m; green solid square, convolution model from Ref. 11; and purple solid circle, measurement from Ref. 11.

component is determined by the trigonometric functions, and the radial component is an integral containing the Bessel functions and an arbitrary excitation velocity profile. The proposed expansion converges much faster than the direct numerical integration of the quasilinear solution.

The numerical results are presented for several steerable PALs and compared to predictions obtained using the convolution model. A comparison with the measurements reported by Shi and Kajikawa¹¹ in Figs. 4, 6, and 8 demonstrates that the proposed cylindrical expansion provides better agreement with the measurement when compared to the convolution model. This is because the complex nonlinear interactions of the ultrasound waves in the near field are correctly captured by the cylindrical expansion. In addition, the proposed cylindrical expansion in Eqs. (19) and (20) can predict the near audio sound field as shown in Sec. IV, whereas it is not applicable for the convolution model in Eq. (6).

The cylindrical expansion requires that the radiation surface of the PAL array is infinitely long in one dimension. This requirement is easy to satisfy because the ultrasonic wavelength is usually much smaller than an ordinary PAL. However, this is not always the case for the audio sound and, therefore, the prediction accuracy at low audio frequencies may deteriorate when using the cylindrical expansion, and this remains to be addressed. Nevertheless, the proposed cylindrical expansion is shown to provide a computationally efficient approach to modelling a PAL after adopting the phased array technique.

ACKNOWLEDGMENTS

This research was supported by the Australian Research Council's Linkage Project funding scheme (Grant No. LP160100616). H.Z. also gratefully acknowledges the financial support by the National Natural Science Foundation of China (Grant No. 11874219).

- ¹W.-S. Gan, J. Yang, and T. Kamakura, "A review of parametric acoustic array in air," *Appl. Acoust.* **73**(12), 1211–1219 (2012).
- ²P. J. Westervelt, "Parametric acoustic array," *J. Acoust. Soc. Am.* **35**(4), 535–537 (1963).
- ³N. Tanaka and M. Tanaka, "Active noise control using a steerable parametric array loudspeaker," *J. Acoust. Soc. Am.* **127**(6), 3526–3537 (2010).
- ⁴C. Shi, Y. Kajikawa, and W.-S. Gan, "Generating dual beams from a single steerable parametric loudspeaker," *Appl. Acoust.* **99**, 43–50 (2015).
- ⁵C. Shi and W.-S. Gan, "Analysis and calibration of system errors in steerable parametric loudspeakers," *Appl. Acoust.* **73**(12), 1263–1270 (2012).
- ⁶C. Shi and W.-S. Gan, "Grating lobe elimination in steerable parametric loudspeaker," *IEEE Trans. Ultrason. Ferroelectr. Freq. Control.* **58**(2), 437–450 (2011).
- ⁷W.-S. Gan, J. Yang, K.-S. Tan, and M.-H. Er, "A digital beamsteerer for difference frequency in a parametric array," *IEEE Trans. Audio Speech Lang. Process.* **14**(3), 1018–1025 (2006).
- ⁸C. Shi, Y. Kajikawa, and W.-S. Gan, "An overview of directivity control methods of the parametric array loudspeaker," *APSIPA Trans. Signal Inf. Process.* **3**, E20 (2014).
- ⁹W.-S. Gan, E.-L. Tan, and S. M. Kuo, "Audio projection: Directional sound and its applications in immersive communication," *IEEE Signal Process. Mag.* **28**(1), 43–57 (2011).
- ¹⁰Y. Hwang, Y. Je, H. Lee, J. Lee, C. Lee, W. Kim, and W. Moon, "A parametric array ultrasonic ranging sensor with electrical beam steering capability," *Acta Acust. united Acust.* **102**(3), 423–427 (2016).
- ¹¹C. Shi and Y. Kajikawa, "A convolution model for computing the far-field directivity of a parametric loudspeaker array," *J. Acoust. Soc. Am.* **137**(2), 777–784 (2015).

- ¹²O. Guasch and P. Sánchez-Martín, "Far-field directivity of parametric loudspeaker arrays set on curved surfaces," *Appl. Math. Model.* **60**, 721–738 (2018).
- ¹³S. I. Aanonsen, T. Barkve, J. N. Tjøtta, and S. Tjøtta, "Distortion and harmonic generation in the nearfield of a finite amplitude sound beam," *J. Acoust. Soc. Am.* **75**(3), 749–768 (1984).
- ¹⁴M. Červenka and M. Bednařík, "A versatile computational approach for the numerical modelling of parametric acoustic array," *J. Acoust. Soc. Am.* **146**(4), 2163–2169 (2019).
- ¹⁵J. Zhong, R. Kirby, and X. Qiu, "The near field, Westervelt far field, and inverse-law far field of the audio sound generated by parametric array loudspeakers," *J. Acoust. Soc. Am.* **149**(3), 1524–1535 (2021).
- ¹⁶G. T. Silva and A. Bandeira, "Difference-frequency generation in nonlinear scattering of acoustic waves by a rigid sphere," *Ultrasonics* **53**(2), 470–478 (2013).
- ¹⁷M. Červenka and M. Bednařík, "Non-paraxial model for a parametric acoustic array," *J. Acoust. Soc. Am.* **134**(2), 933–938 (2013).
- ¹⁸J. Zhong, R. Kirby, and X. Qiu, "A spherical expansion for audio sounds generated by a circular parametric array loudspeaker," *J. Acoust. Soc. Am.* **147**(5), 3502–3510 (2020).
- ¹⁹J. Zhong, R. Kirby, and X. Qiu, "A non-paraxial model for the audio sound behind a non-baffled parametric array loudspeaker (L)," *J. Acoust. Soc. Am.* **147**(3), 1577–1580 (2020).
- ²⁰C. Ye, M. Wu, S. Wu, C. Huang, and J. Yang, "Modeling of parametric loudspeakers by Gaussian-beam expansion technique," *Jpn. J. Appl. Phys.* **49**(7S), 07HE18 (2010).
- ²¹M. Červenka and M. Bednařík, "On the structure of multi-Gaussian beam expansion coefficients," *Acta Acust. united Acust.* **101**(1), 15–23 (2015).
- ²²T. Kamakura, N. Hamada, K. Aoki, and Y. Kumamoto, "Nonlinearly generated spectral components in the nearfield of a directive sound source," *J. Acoust. Soc. Am.* **85**(6), 2331–2337 (1989).
- ²³J. Zhong, S. Wang, R. Kirby, and X. Qiu, "Reflection of audio sounds generated by a parametric array loudspeaker," *J. Acoust. Soc. Am.* **148**(4), 2327–2336 (2020).
- ²⁴J. Zhong, S. Wang, R. Kirby, and X. Qiu, "Insertion loss of a thin partition for audio sounds generated by a parametric array loudspeaker," *J. Acoust. Soc. Am.* **148**(1), 226–235 (2020).
- ²⁵H. O. Berktaý, "Possible exploitation of non-linear acoustics in underwater transmitting applications," *J. Sound Vib.* **2**(4), 435–461 (1965).
- ²⁶H. O. Berktaý and D. J. Leahy, "Farfield performance of parametric transmitters," *J. Acoust. Soc. Am.* **55**(3), 539–546 (1974).
- ²⁷C. Shi and W.-S. Gan, "Product directivity models for parametric loudspeakers," *J. Acoust. Soc. Am.* **131**(3), 1938–1945 (2012).
- ²⁸M. B. Moffett and R. H. Mellen, "Nearfield characteristics of parametric acoustic sources," *J. Acoust. Soc. Am.* **69**(2), 404–409 (1981).
- ²⁹T. Mellow and L. Kärkkäinen, "On the sound fields of infinitely long strips," *J. Acoust. Soc. Am.* **130**(1), 153–167 (2011).
- ³⁰M. A. Poletti, "Cylindrical expansions of sound radiation from resilient and rigid infinite strips with reduced error," *J. Acoust. Soc. Am.* **145**(5), 3104–3115 (2019).
- ³¹T. D. Mast and F. Yu, "Simplified expansions for radiation from a baffled circular piston," *J. Acoust. Soc. Am.* **118**(6), 3457–3464 (2005).
- ³²J. Zhong and X. Qiu, "On the spherical expansion for calculating the sound radiated by a baffled circular piston," *J. Theor. Comput. Acoust.* **2020**, 2050026.
- ³³M. Červenka and M. Bednařík, "Parametric acoustic array lensed by a gradient-index phononic crystal," *J. Acoust. Soc. Am.* **149**(6), 4534–4542 (2021).
- ³⁴E. G. Williams, *Fourier Acoustics: Sound Radiation and Nearfield Acoustical Holography* (Academic, San Diego, CA, 1999).
- ³⁵S. Zhang and J. Jin, *Computation of Special Functions* (Wiley, New York, 1996).
- ³⁶ISO 9613-1:1993, "Acoustics—Attenuation of sound during propagation outdoors—Part 1: Calculation of the absorption of sound by the atmosphere" (International Organization for Standardization, Genève, Switzerland, 1993).
- ³⁷M. Majić and E. C. Le Ru, "Numerically stable formulation of Mie theory for an emitter close to a sphere," *Appl. Opt.* **59**(5), 1293–1300 (2020).